COMPARISON OF ADAPTIVE INPUT OUTPUT FEEDBACK LINERIZATION TECHNIQUE WITH ANN BASED CONTROL FOR LINEAR INDUCTION MOTORS

[1]BODDU MURALI MOHAN
Student, dept. of Electrical and Electronics Engineering, JNTUA Anantapuram.

Abstract— this paper proposes a neural based full-order Luenberger Adaptive speed observer for sensorless linear induction motor (LIM) drives, where the linear speed is estimated on the basis of the linear neural network: TLS EXIN neuron. With this reference, a novel state space-vector representation of the LIM has been deduced, taking into consideration the so-called end effects. Starting from this standpoint, the state equation of the LIM has been discretized and rearranged in a matrix form to be solved by a least-square technique. The TLS EXIN neuron has been used to compute on-line, in recursive form, the machine linear speed since it is the only neural network able to solve on-line in a recursive form a total least-squares problem. The proposed TLS full order Luenberger Adaptive speed observer has been tested MATLAB Simulation on suitably developed test setup.

Keywords — Linear Induction Motor (LIM), End effects, State Model, Luenberger Observer, Total Least-Squares, Neural Networks

I. INTRODUCTION

Literature about linear induction motor (LIM) is huge [1][2]. The option that LIMs offer to develop a direct linear motion without the need of any gear-box for the motion transformation (from rotating to linear) has been the key issue for their study. The counterpart of this potential advantage is the increase of complexity of the machine model, which presents the so-called end effects and border effects. These effects, which are due to the absence of a cylindrical symmetry in the inductor structure with respect to the rotating machine, both in the longitudinal and in the transversal direction, make obtaining good performance from the linear drive a difficult task. Speed control of the LIM, however, requires the adoption of a linear encoder, which is typically more expensive and less reliable of the corresponding counterpart in the rotating machine.

As a matter of fact, in the LIM case, the cost of the encoder increases with the length of the induced part track, which could be very demanding in applications like railway traction systems and in general movement systems with long tracks. The possibility of adopting suited sensorless techniques [3][4] is thus very interesting for these applications, where typically the linear encoder would also be exposed to potentially damaging environmental factors (sun, humidity, mechanical stress etc.). Very few applications of sensorless techniques suited for LIMs have been proposed in literature, among which [5][6], probably because of the further increased complexity of a speed observer which should consider also the end effects of the machine. In particular, [5] proposes a complex adaptive speed sensorless controller for the LIM, while [6] proposes a sensorless technique suited for LIMs based on high frequency signal injection. In general signal injection techniques reveal difficult to be applied to LIMs, since there is no slotting effect in the induced part track and even the saturation of the main flux is hard to be tracked. [7][8] Propose a neural based MRAS observer, where the adaptive model is a linear neural network, respectively in MATLAB Simulation.

This paper proposes a neural based full-order Luenberger Adaptive speed observer, where the linear speed is estimated on the basis of linear neural network: the TLS EXIN neuron. With this reference, a novel state space-vector representation of the LIM has been deduced, taking into consideration the LIM end effects. Starting from this standpoint, the state equations of the LIM have been discredited and rearranged in a matrix form to be solved by a least-square technique. The TLS EXIN neuron has been used to compute on-line, in recursive form, the machine linear speed since it is the only neural network able to solve on-line in a recursive form a total least-squares problem. The proposed TLS full-order Luenberger Adaptive speed observer has been tested on suitably developed test setup. This observer is the extension to LIMs of the already proposed TLS full-order Luenberger speed observer, initially developed for RIMs [9][10]. It is not, however, simply the application of the former technique to a linear motor, but the entire state space-vector model, which is the core of the observer, has been analytically inferred to take into consideration the end effects, making the observer suitable to LIM drives.

II. MODELING OF IM FOR DTC

The mathematical model of an IM in the stationary reference frame can be written as

$$\begin{bmatrix} v_{s\alpha} \\ v_{s\beta} \\ 0 \\ 0 \end{bmatrix} = \begin{bmatrix} R_S + pL_s & 0 & pL_m & 0 \\ 0 & R_S + pL_s & 0 & pL_m \\ pL_m & P\omega_m L_m & R_r + pL_r & P\omega_m L_r \\ -P\omega_m L_m & pL_m & -P\omega_m L_r & R_r + pL_r \end{bmatrix} + \begin{bmatrix} i_{s\alpha} \\ i_{s\beta} \\ i_{rd} \\ i_{rq} \end{bmatrix} . \quad (1)$$

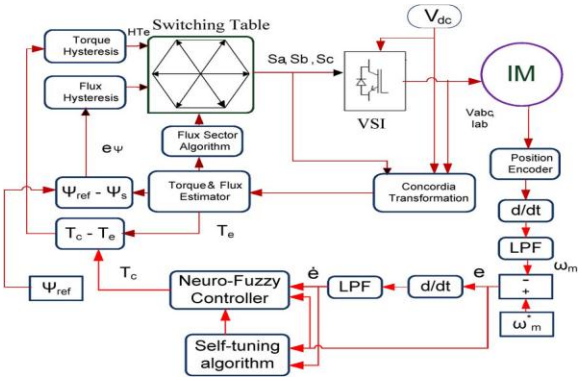

Fig. 1. NFC-based DTC scheme for IM drive.

The proposed NFC-based DTC scheme for IM drive is shown in Fig. 1. The output voltage of a three-phase voltage source inverter (VSI) or the input to the stator of the IM is given by

$$V_{sa} = \frac{V_{\rm dc}}{3}(2S_a - S_b - S_c) \qquad (2\text{-a})$$

$$V_{sb} = \frac{V_{\rm dc}}{3}(2S_b - S_c - S_a) \qquad (2\text{-b})$$

$$V_{sc} = \frac{V_{\rm dc}}{3}(2S_c - S_a - S_b). \qquad (2\text{-c})$$

The real and imaginary parts of the stator voltage vector are obtained by using the Concordia transformation as

$$\begin{bmatrix} V_{s\alpha} \\ V_{s\beta} \end{bmatrix} = \begin{bmatrix} 1 & 1/2 & 1/2 \\ 0 & \sqrt{3}/2 & \sqrt{3}/2 \end{bmatrix} \begin{bmatrix} V_{sa} \\ V_{sb} \\ V_{sc} \end{bmatrix}. \qquad (3)$$

The motor-developed torque is given by

$$T_e = \frac{3}{2}P[\psi_{s\alpha}I_{s\beta} - \psi_{s\beta}I_{s\alpha}]. \qquad (4)$$

The stator flux angle, flux vector, and its components are given by

$$\theta_s = \tan^{-1}(\psi_{s\beta}/\psi_{s\alpha}) \qquad (5.a)$$

$$\psi_s = \sqrt{\psi_{s\alpha}^2 + \psi_{s\beta}^2} \qquad (5.b)$$

$$\psi_{s\alpha} = \int (V_{s\alpha} - R_s I_{s\alpha})dt \qquad (6.a)$$

$$\psi_{s\beta} = \int (V_{s\beta} - R_s I_{s\beta})dt. \qquad (6.b)$$

The well-known problems associated with the real-time implementation of the pure integral in (6.a) and (6.b) are easily overcome by modifying the integral as follows :

$$\psi_{s\alpha} = \int \{[1 - j\lambda \text{sign}(w)]\,(V_{s\alpha} - R_s I_{s\alpha}) - \lambda|w|\psi_{s\alpha}\}dt \quad (7.a)$$

$$\psi_{s\beta} = \int \{[1 - j\lambda \text{sign}(w)]\,(V_{s\beta} - R_s I_{s\beta}) - \lambda|w|\psi_{s\beta}\}dt. \quad (7.b)$$

Based on the simulation tests, the value of λ is optimized to 3.1. The two digits produced by the hysteresis comparators and one digit produced by the flux position are collectively used to trigger the switches of the VSI which selects the appropriate voltage vector by using the classical DTC lookup table. The block diagram of the proposed NFC-based DTC scheme incorporating the hysteresis band adaptation for IM drive is shown in Fig. 1.

III SIMULATION RESULTS SIMULINK DIAGRAM

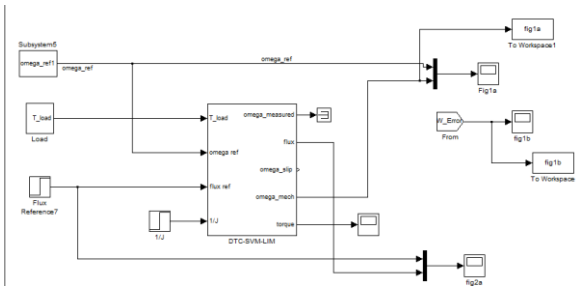

The proposed adaptive FL control technique taking into consideration the LIM dynamic end-effects, with integrated on-line estimation of the parameter α, has been tested in both numerical simulation and experimentally. The aim of the numerical simulations is to show some important results, among which the co-herence between simulation and experiments. Moreover, some tests can be made only in numerical simulation because of con-straints of the experimental set-up. This is the case of high speed (rated speed of about 5 m/s) tests. As a matter of fact, such test cannot be made experimentally because of the limited length of the induced part track (1.6 m). For this reason the high speed test has been carried out by simulation, and the tests at lower speed have been carried out both experimentally and by means of simulations in order to compare with the obtained experimental results. A further scope of adopting numerical simulation is to prove the effectiveness of the proposed approach; in fact, by means of simulations it is possible to show the convergence of the adaptation algorithm of the induced-part time constant as well as its accuracy in the estimation. On the contrary, it cannot be done experimentally due to the fact that the induced-part time is unknown and unmeasurable.

Numerical simulations have been performed in Matlab® – Simulink ®environment. With this regard, the dynamic model of the LIM including its end-effect, the adaptive FL control technique, the flux model and the inverter model controlled by its SV-PWM (Space-Vector Pulse-Width Modulation) technique, have been purposely developed. With regard to the LIM dynamic model used as "machine under test", the model proposed and validated in Pucci (2014) both by means of finite element analysis and ex-perimentally has been adopted.

To demonstrate the advantages of the adoption of the proposed adaptive FL, it has been compared to the FL control technique pro-posed in Alonge et al. (2015b), which does not present any robustness versus any parameters' variation. As a matter of fact, whenever the α estimation feature is not activated by the control system occurring when the estimated $\alpha^{\tilde{}}$ coincides with the corresponding one of the LIM, the proposed FL coincides with Alonge et al. (2011a).

The first test consists in a speed step from 0 to 5 m/s (t¼1 s) followed by a speed reversal 5 to 5 m/s (t¼5 s) at no load. Contemporary to the first speed step, a t¼1 s, a $|\psi_r|$ step variation from 0 to 0.6 Wb (rated flux) is commanded. The LIM has been operated so that, at the beginning, the value of $\alpha^{\tilde{}}$ provided to the FL controller is twice the value of the real machine (detuning of the FL controller) which is a very challenging working condition, very rarely encountered in the real world practice. It should be further noted that, in such tests, the flux model used to estimate $|\psi_r|$ is adapted on-line coherently with the FL controller, in accordance with the current estimation of α. Fig. 1 shows the reference and real speed, speed tracking error during such a test. Fig. 2 shows the corresponding waveforms of the reference and real $|\psi_r|$, flux tracking error, Fig. 3 shows the corresponding waveforms of the i_{sx},

i_{sy} inductor currents and, finally, Fig. 4 shows the corresponding waveforms of the reference and estimated $\alpha^{\sim}$, as well as the esti-mation tracking error. The figure of the estimated $\alpha^{\sim}$ clearly high-lights that the FL controller is initially completely detuned as far as the knowledge of such parameter is concerned. After t¼1 s, when the first speed step reference occurs, the estimated $\alpha^{\sim}$ correctly tracks the real one of the machine; correspondingly its estimation errors converge to zero. It should be noted that the algorithm is able to track the correct value of the parameter, starting from its wrong knowledge, even if the real parameter varies during the estimation process. This is a peculiarity of such a technique when applied to the LIM case, because L_r varies with the machine speed because of the dynamic end-effects independently from the magnetizing level of the machine. Such a complication does not exist in the RIM case, where L_r can be assumed to be constant independently from the speed if the flux level is maintained constant. Coherently with the $\alpha^{\sim}$ adaptation law in (30), the esti-mated parameter is adapted on-line only in the presence of al-ternatively a flux tracking error or in the presence of a load. When the speed reversal occurs, at t ¼5 s, the estimated $\alpha^{\sim}$ tend to track

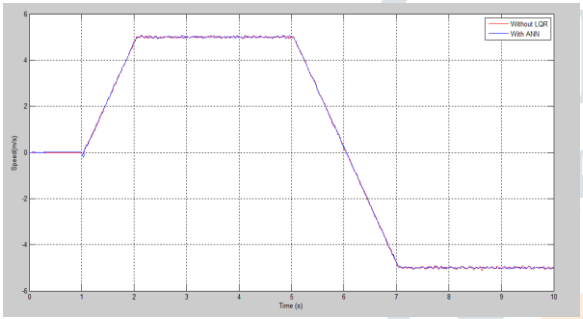

Fig. 1. Reference and real speed, speed tracking error during a speed step 0 → 5 m/s followed by a speed reversal 5 → − 5 m/s at no load (simulation).

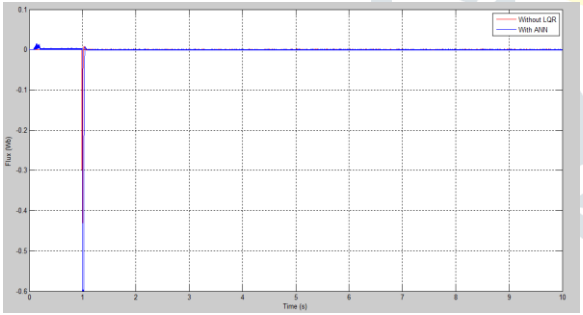

Fig. 2. Reference and real flux followed by a speed reversal $|\psi_r|$, flux tracking error during a speed step 0 → 5 m/s 5 → − 5 m/s at no load (simulation).

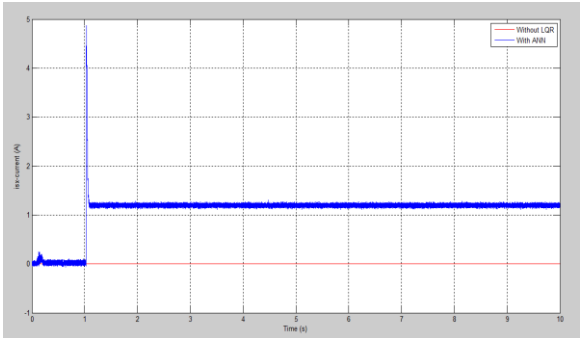

Fig. 3. i_{sx}, i_{sy} inductor currents during a speed step 0 → 5 m/s followed by a speed reversal 5 → − 5 m/s at no load (simulation).

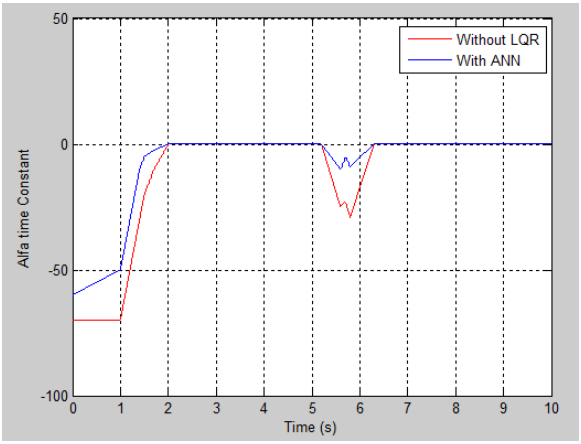

Fig. 4. Reference α and estimated $\alpha^{\sim}$, estimation tracking error during a speed 0 → 5 m/s followed by a speed reversal step 5 → − 5 m/s at no load (simulation).

The real one, but its dynamics is slower than that of the real parameter, which is governed by the speed loop dynamic. During the speed transient, the controller is thus only partially tuned, while at the end of the transient the estimated $\alpha^{\sim}$ converges to the real value of the machine. It should be further noted that differ-ently from Alonge et al. (2015b) and Pucci (2012) where the var-iation law of the L_m with the speed had been assumed correctly modelled and known a priori (with the related approximations), here such a variation is estimated on-line. This is a particularly interesting characteristics of such an approach, different from that in Alonge et al. (2015a, 2015b) where the variation law of the parameters versus the LIM speed had been assumed perfectly a priori known. As a matter of fact, however, the above mentioned variation law, even if well approximated, presents some limits. Such limits are overcome here thanks to the on-line estimation of the variability of such parameters with the LIM speed.

Correspondingly, Fig. 1 shows that the FL controller permits us to suitably control the speed during the entire test, with the speed tracking error converging to zero quickly at the end of each speed transient. Same considerations can be made for the $|\psi_r|$ waveform, which correctly tracks its reference with zero steady-state tracking error, thanks to the on-line $\alpha^{\sim}$ estimation feature. Coherently with what stated above, the flux presents a non-null tracking error during speed transient, caused by the variation of L_r with the LIM speed which is estimated on-line, and not a priori established as in Alonge et al. (2015b) and Pucci (2012). Finally, the i_{sx}, i_{sy} waveforms are co-herent with the speed and flux waveforms. In particular, i_{sx} is main-tained at a constant value, because the magnetization level of the machine is maintained constant. On the other hand, i_{sy} exhibits step-wise waveform, which is proportional to the electromagnetic force. It must be noted that, during the speed transients, i_{sy} presents some oscillations. Such oscillations are caused by the fact that $\alpha^{\sim}$ presents a non-null estimation error during transients, causing a non-perfect field orientation during transients, caused by the LIM end-effects.

Figs. 5–8 show the same kind of waveforms, obtained under constant LIM speed operation set at 5 m/s and constant induced part flux amplitude set at 0.6 Wb. The LIM is initially operated at no-load, while at t¼5 s a load step load force of amplitude 80 N is applied. As in the first test, the LIM has been operated so that, at the beginning, the value of $\alpha^{\sim}$ provided to the FL controller is twice the value of the real machine (detuning of the FL controller). Fig. 8 clearly highlights that, coherently with the $\alpha^{\sim}$ adaptation law in (30), the estimated parameter is adapted on-line only in the pre-sence of the application of the load force. During the first 5 s, at no load

conditions, the FL controller remains detuned. On the con-trary, at t ¼5 s, the estimated $\alpha\tilde{}$ converges quickly towards its real value, guaranteeing the correct field orientation conditions. At the same time, the speed waveform exhibits a very fast dynamics, with a peak value of speed tracking error which is very limited, even during the contemporary convergence process of $\alpha\tilde{}$. Even the $|\psi_r|$ waveform correctly tracks its reference with zero steady-state tracking error, thanks to the on-line $\alpha\tilde{}$ estimation feature.

Finally, the i_{sx}, i_{sy} waveforms are coherent with the speed and flux waveforms. In particular, i_{sx} is maintained at a constant value, be-cause the magnetization level of the machine is maintained constant. On the other hand, i_{sy} exhibits a step-wise waveform, which is pro-portional to the electromagnetic force. As recalled above for the first test, during the speed transients, i_{sy} presents some oscillations, whose interpretation has already been given above.

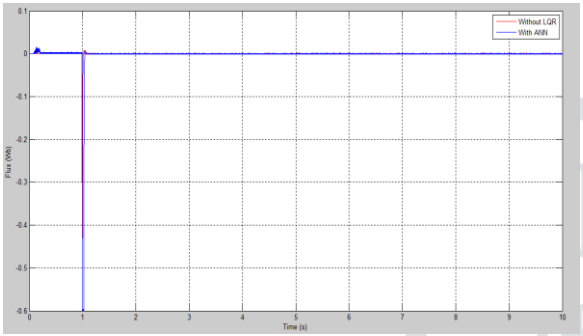

Fig. 6. Reference and real flux $|\psi_r|$, flux tracking error with v¼5 m/s, $|\psi_r|$ = 0.6 Wb when a step load force equal to 80 N is applied (simulation)

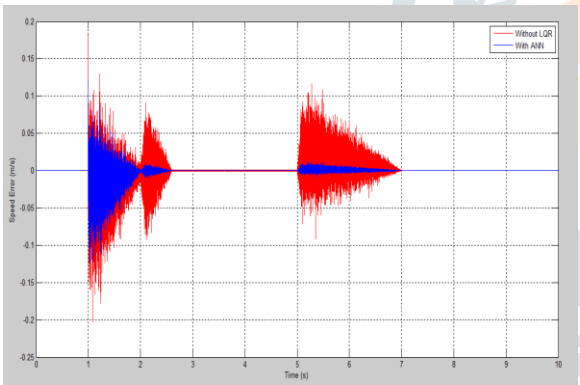

Fig. 7. Reference α and estimated $\alpha\tilde{}$, estimation tracking error with v¼5 m/s, $|\psi_r|$ = 0.6 Wb when a step load force equal to 80 N is applied (simulation).

0.6 Wb has been given to the drive. At t¼2.5 s a speed step re-ference of 0.2 m/s has been given at no load. As in the previous tests, at the beginning, the value of $\alpha\tilde{}$ provided to the FL controller is different from the value of the real machine. Fig. 12 clearly highlights that, coherently with the $\alpha\tilde{}$ adaptation law in (30), the estimated parameter is adapted on-line firstly during the initial flux transient and secondly during the speed transient. The speed waveform exhibits a very fast dynamics, even during the con-temporary convergence process of $\alpha\tilde{}$. Even the $|\psi_r|$ waveform, shown in Fig. 10, correctly tracks its reference with zero steady-state tracking error, thanks to the on-line $\alpha\tilde{}$ estimation feature. Finally, the i_{sx}, i_{sy} waveforms, shown on fig 6, are coherent with the speed and flux waveforms. In particular, i_{sx} is maintained at a constant value, because the magnetization level of the machine is maintained constant. On the other hand, i_{sy} exhibits a step-wise waveform, which is proportional to the electromagnetic force.

CONCLUSIONS

This paper proposes a neural based full order Luenberger Adaptive speed observer for linear induction motor (LIM) drives, where the linear speed is estimated on the basis of linear neural network: the TLS EXIN neuron. With this reference, a novel state space-vector representation of the LIM has been deduced, taking into consideration the LIM end effects. Starting from this standpoint, the state equation of the LIM has been discretized and rearranged in a matrix form to be solved by a least-square technique. The TLS EXIN neuron has been used to compute on-line, in recursive form, the machine linear speed since it is the only neural network able to solve on-line in a recursive form a total least-squares problem. The proposed TLS full-order Luenberger Adaptive speed observer has been tested experimentally on suitably developed test setup. Results show that the sensorless LIM drive is able to work properly, with low speed estimation error, at very low speed (2% of the rated speed) and zero speed.

REFERENCES

[1] I. Boldea, S. Nasar, *Linear Electric Motors*, Prentice-Hall inc., 1987.

[2] I. Boldea, S. A. Nasar, *Linear Electric Actuators and Generators*, Cambridge University Press, 1997.

[3] K. Rajashekara, A. Kawamura, K. Matsuse, *Sensorless Control of AC Motor Drives*, IEEE Press, 1996.

[4] Holtz, " Sensorless control of induction motor drives", *Proceedings of the IEEE*, Volume: 90 , n° 8 , pp. 1359-1394, Aug. 2002.

[5] Chin-I Huang, Fu Li-Chen, Wen-Yuh Jywe, and Jing Chung Shen, "Speed motion-sensorless with adaptive control approach of linear induction motor unknown resistance and payload", *IEEE Trans. Ind. Appl.*, pp. 3887 _ 3893, 15-19 June 2008.

[6] Hybng-Min Ryu, Jug-Ik Ha, and Seung-Ki Sul, "A New sensorless control thrust control of linear induction motor", *Conference Record of the 2000 IEEE Industry Applications Conference, 2000*, Vol. 3, pp. 1655 - 1661 vol.3.

[7] M. Cirrincione, M. Pucci, A. Sferlazza, G. Vitale, "Neural based MRAS Sensorless Techniques for High Performance Linear Induction Motor Drives", *36th Annual Conference of the Industrial Electronics Society, (IECON 2010)*, 7-10 November, Phoenix, USA.

[8] A. Accetta, M. Cirrincione, M. Pucci, G. Vitale, "MRAS Speed Observer for High Performance Linear Induction Motor Drives based on Linear Neural Networks", *IEEE Transactions on Power Electronics*, in press.

[9] M. Cirrincione, M. Pucci, G. Cirrincione, G. Capolino, "An Adaptive Speed Observer Based on a New Total Least-Squares Neuron for Induction Machine Drives", *IEEE Transactions on Industry Applications*, vol. 42, n.1, January/February 2006, pp.89-104.

[10] M. Cirrincione, M. Pucci, G. Cirrincione, G. Capolino, "Sensorless Control of Induction Machines by a New Neural Algorithm: the TLS EXIN Neuron", *IEEE Transactions on Industrial Electronics*, vol. 54, n. 1, February 2007, Special Section: Neural Network Applications in Power Electronics and Motor Drives (Guest Editor B.K. Bose).

[11] J. Duncan, C. Eng., "Linear induction motor-equivalent-circuit model", *Proc. IEE*, Vol. 130, Pt. B, No. 1, pp. 51-57, 1983.

[12] H. Kubota, K. Matsuse and T. Nakano, "DSP-Based Speed Adaptive Flux Observer of Induction Motor", *IEEE Transactions on Industry Applications*, Vol. 29, n° 2, pp. 344-348, March/April 1993.

[13] G. Cirrincione, M. Cirrincione, J. Hérault and S. Van Huffel, "The MCA EXIN Neuron for the Minor Component Analysis: Fundamentals and Comparisons," *IEEE Transactions on Neural Networks* , January 2001.

[14] G. Cirrincione, M. Cirrincione, *Neural-Based Orthogonal Data Fitting: The EXIN Neural Networks*, John Wiley and Sons, Inc., 2010.

[15] J.H. Sung, and K. Nam "A New Approach to Vector Control for a Linear Induction Motor Considering End Effects ", *IEEE IAS 1999*, pp. 2284 - 2289 vol.4.

[16] G. Kang, K. Nam, "Field-oriented control scheme for linear induction motor with the end effect", *IEE Proc.-Electr. Power Appl.*, Vol. 152, No. 6, November 2005.

[17] V. Isastia, G. Gentile, S. Meo, A. Ometto, N. Rotondale, M. Scarano, "A voltage feeding algorithm for vectorial control of linear asynchronous machines taking into account end effect", *Power Electronic Drives and Energy Systems for Industrial Growth*, 1998. Vol.2, pp. 729-734.

[18] I. Takahashi and Y. Ide, "Decoupling Control of thrust and attractive force of a LIM using a space vector control inverter", *IEEE Trans. Ind. Appl.*, vol. 29, 1993, pp. 161-167.